# RETLab: A fast design-automation framework for arbitrary RET networks

Mohammad D. Mottaghi, Arjun Rallapalli, Chris Dwyer
Duke University – Durham, NC, USA
Email: mamad@cs.duke.edu, {arjun.rallapalli, dwyer}@ece.duke.edu

***Abstract*** [1] **—Resonance energy transfer (RET) circuits are networks of photo-active molecules that can implement arbitrary logic functions. The nanoscale size of these structures can bring high-density computation to new domains, e.g., in vivo sensing and computation. A key challenge in the design of a RET network is to find, among a huge set of configurations (i.e., design space), the optimum choice and arrangement of molecules on a nanostructure. The prohibitively large size of the design space makes it impractical to evaluate every possible configuration, motivating the need for design-space pruning to be integrated into the design flow. To this end, we have developed a computer-aided design framework, called *RETLab*, that enables structured pruning of the design space to extract a sufficiently small subset, which is fully evaluated and ranked based on user-defined metrics to yield the best configuration. More importantly, we have developed a new RET-simulation algorithm, which is several orders of magnitude (e.g., for a 4-node network, one million times) faster than the conventional Monte-Carlo-based simulation (MCS). This speedup in configuration evaluation enables a significantly more extensive design-space exploration with fewer and less constrained heuristics, compared to existing RET-network design methods which are ad-hoc and rely on MCS for configuration evaluation.**

***Keywords— design space; candidate space; sample space; fluorescence; RET network; FRET; chromophores; RET logic***

## I. INTRODUCTION

In a class of photo-active molecules, called *chromophores*, photon absorption creates an *exciton* which is a transient state that can migrate from one molecule to another nearby molecule through a mechanism called Förster Resonance Energy Transfer (FRET)[1]. The control of exciton currents in a network of these chromophores (RET network) enables logic functionality, in the same fashion the control of *electron* currents enables logic functionality in electronic circuits[2]. Such nanoscale logic devices may offer a way to realize unconventional computing paradigms which require computational elements to function in many kinds of organic environments such as in ubiquitous or swarm computing. Furthermore, RET devices are biocompatible and can be used in applications which require biological environments, such as *in vivo* sensing [3, 4] and targeted drug delivery.

A RET network can be represented by an Exciton Flow Graph (EFG) in which nodes represent a set of desired photo-physical properties and edge weights are inter-node distances. The realization of an EFG faces two challenges in practice: first, the underlying nanostructure that hosts the chromophores does not allow arbitrary positions for the chromophores. Instead, it allows the chromophore molecules to attach (i.e., form a covalent bond) only to a set of particular sites, rendering some inter-node distances unrealizable on the nanostructure. Further, because of the highly-*nonlinear* nature of RET networks the required distance cannot be approximated to the closest possible one, either. Second, when a *real* chromophore is chosen to represent an *ideal* chromophore required by EFG, some undesired photo-physical properties are imposed on the network by the molecular structure of the real chromophore; for example, an ideal chromophore only absorbs photons of a particular wavelength range, while not absorbing any out-of-range photons, whereas, a commercially available chromophore type (also called dye) often has a wide range of wavelength absorption and thus, absorbs (although rarely) out-of-range photons, as well. These two challenges cause a gap between the desired- and real behavior of a manufactured RET network, the minimization of which is among the objectives of the design process.

Finding the optimum configuration (i.e., dye and site assignment to every network node) is complicated by the highly-nonlinear nature of chromophore interactions; specifically, the lack of an efficient (polynomial time) and yet function-independent algorithm for this purpose has lead all existing RET-network design methods to be *ad hoc* and specific to RET networks with particular functionalities (e.g., wire [5, 6], light-harvesting [7], logic [8, 9], etc.). The drawback of these *ad hoc* methods is their lack of generalizability to RET networks with different functionalities, as well as their poor design-space exploration capabilities which is exacerbated by the inherently-slow nature of their design flow.

In this paper, we present an automated design framework that addresses these issues. Specifically, we have made the following contributions:

1- By decoupling the functionality aspects of RET-network design from its fabrication issues, we have developed a function-independent high-throughput automated design framework for RET logic.
2- We have also developed a novel configuration evaluation algorithm which is multiple orders of magnitude faster than conventional evaluation methods.

The rest of the paper is organized as follows: In section 2 the theoretical background of RET logic is explained and in section 3, the RETLab architecture is presented. The new configuration-evaluation algorithm is described in section 4

[1] 978-3-9815370-2-4/DATE14/©2014 EDAA

followed by the evaluation and discussion in section 5, and finally, the conclusion in section 6.

## II. Background: RET Circuits

In order for a RET network to exhibit a consistent behavior, its chromophores have to be fixed in position relative to one another and this is achieved by attaching them to an underlying nanostructure which could be a DNA grid[10] or a protein or any other supramolecular structure. Therefore each structure holds a fixed number of chromophores (of different types), and a relatively large population of these multi-chromophore structures (e.g. 250 nano moles) constitutes a RET device which in turn performs a logic function under certain excitation conditions.

A chromophore is normally in its ground state, i.e., at energy equilibrium with its micro environment, until it absorbs a photon which promotes it to an excited state. Since the excited state is unstable the excited molecule relaxes back to its ground state after a period of time [11]. In general, an excited molecule de-excites (i.e., relaxes back to its ground state) through one of these pathways: 1- Emitting a photon (called *fluorescence*), 2- Transferring energy to a nearby and unexcited chromophore (called *RET*), or 3- Releasing the excess energy non-radiatively, which we call exciton-loss. Förster Resonance Energy Transfer (FRET or RET) is a mechanism through which an excited molecule (called donor) de-excites by transferring its excess energy to an unexcited nearby acceptor molecule [11].

When a fraction of a chromophore's population (denoted by [D]) is excite, all these relaxation pathways compete with one another simultaneously at different rates to depopulate the excited population (denoted by [D*]) as described by Eq.1 wherein $k_F$, $k_L$, and $k_R$ are the rate-constants of fluorescence, loss, and RET, respectively.

$$\frac{d[D^*]}{dt} \equiv D' = -[D^*](k_F + k_L + k_R) \qquad (1)$$

### A. Implementation of Logic Functions

Each chromophore is maximally excited at a particular wavelength ($\lambda_{ex}$) and fluoresces at a longer wavelength ($\lambda_{em}$) after an average of $\tau$ units of time (called lifetime) [1]. The photo-physical properties of chromophores depend on their type, i.e., molecular structure. Many different chromophore types (also called dyes) are commercially available; for example, *Lucifer Yellow* is a dye with $\lambda_{ex}$=428nm and $\lambda_{em}$=535nm, and *Texas Red* is another dye with different properties: $\lambda_{ex}$=589nm and $\lambda_{em}$=615nm. The lifetime ($\tau$) values for these dyes are 5.7ns and 4.2 ns respectively[2].

The absorption and emission of photons by chromophores can serve as the input and output mechanisms, respectively. Signal separation is achieved by wavelength division multiplexing (WDM) in the same physical medium (channel). For example, Fig. **1** shows an OR gate in which two different dyes are used for A and B and therefore each one gets excited by a different wavelength ($\lambda_{ex(A)}$ and $\lambda_{ex(B)}$). The communication is enabled by RET, the rate (strength) of which can be tuned by adjusting the donor-acceptor distance or the choice of corresponding dyes. In the OR gate example (Fig. 1), A and B have RET to O and therefore an exciton in either one of them hops to O and eventually fluoresces out (at $\lambda_O$) which can be detected by a photo-detector.

In general arbitrary logic functions can be implemented by controlling the *exciton flow* within a RET network, which is achieved by either engineering pairwise RET rates, or saturating acceptors. The rate constant ($k_R$) of a RET pair depends non-linearly on the donor-to-acceptor distance as well as their molecular structures as expressed by Eq.2 [11]:

$$k_R = \frac{1}{\tau_0}\left(\frac{R_0}{r}\right)^6 \qquad (2)$$

In this equation, $R_0$ is called the Förster radius which is the distance at which half of the excited donors transfer to their acceptors[11]. Depending on their molecular structure, different donor-acceptor pairs have different $R_0$ values. Further, $\tau_0$ is the intrinsic excited-state lifetime of the donor.

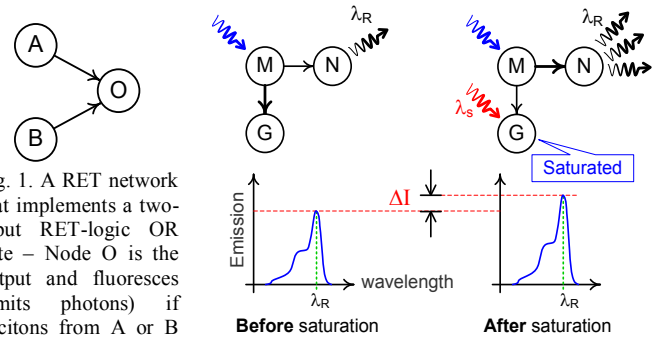


Fig. 1. A RET network that implements a two-input RET-logic OR gate – Node O is the output and fluoresces (emits photons) if excitons from A or B hop to O through RET.

Fig. 2. Saturation of G weakens the M→G path and increases the fluorescence of N

Another exciton-flow control mechanism is acceptor saturation which can be achieved by *intensely* exciting the acceptor either through another donor or directly by incident photons. Acceptor saturation occurs because *only a single* exciton can excite an unexcited chromophore, and no excitons can hop to an already-excited chromophore [12]. This implies that when multiple excitons attempt to hop to the *same* acceptor simultaneously, *exciton collision* occurs as a result of which only one exciton hops, while others remain unmoved. In Fig. 2 for example, nodes G and N compete to depopulate the excited M population. The saturation of G induces an increase on N's share of hopping excitons from M, because after being saturated, G receives fewer excitons from M, leaving more excitons available for N to receive per unit time.

## III. Proposed Automated Design Framework

One of the drawbacks of existing RET-network design methods is their low throughput which, with a limited design time, translates to poor and coarse-grained exploration of the design space. The key to overcome this problem is higher throughput which we have achieved by making two modifications to existing RET design flows: first, we have added a *validation* step before the evaluation step, which quickly identifies disqualified configurations without thorough

[2] Excitation, emission and lifetime data are reported by the iss website.

simulation. Second, we have developed a new evaluation algorithm which is faster than existing evaluation algorithms.

### A. Overview

As illustrated in Fig. 3, the proposed design flow involves user-guided sampling of the design space followed by validation of each sample to check if it qualifies for a potential solution (candidate). In this figure, the design space is the set of all possible configurations (i.e., dye-site assignments) and the sample space is a subset of the design space for every vector of which a quick inspection is performed. Those vectors out of the sample space which pass the validation test (quick inspection) form the candidate space. To find the final solution, all (or some) candidates are fully simulated, from the results of which the values of a set of user-defined metrics (response) are extracted. Finally the candidates are ranked based on these metrics and the Pareto optimal configuration is chosen as the solution(s).

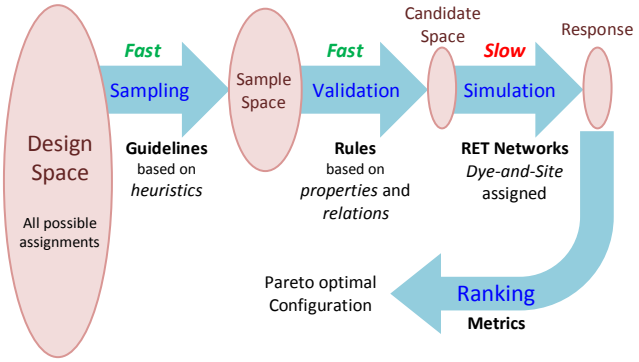


Fig. 3. Overview of the proposed design flow – four major steps: sampling, validation, simulation and ranking

In general, the output quality, as well as the running time of the design process is highly influenced by the domain-specific step of sampling. As shown in Fig. **4**, most parts of the design space, due to its prohibitively-large size, cannot even be sampled. In fact, *guided* by a set of user-provided heuristics, RETLab samples *only* those regions of the design space that are likely to contain a candidate.

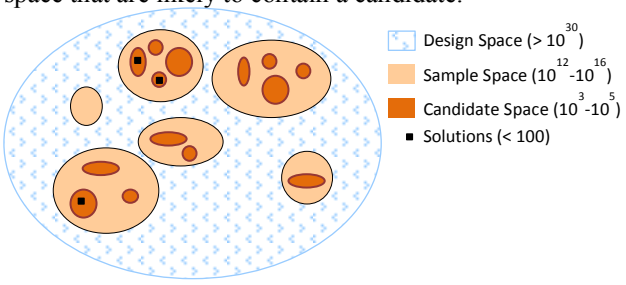


Fig. 4. Relative size of the design space vs. sample space and candidate space – Most regions of the design space are not inspected (sampled).

To accurately compare two configurations, they both have to be simulated in detail. However, many configurations can be easily disqualified if they violate certain circuit-specific rules the checking of which, compared to circuit simulation, is appreciably faster. Therefore, the *validation* step has been added to the design flow with the purpose of improving the overall throughput by avoiding many unnecessary and relatively-slow detailed simulations of unqualified configurations; for instance in Fig. **1**, the A-to-B distance must be more than 5nm (i.e. $|A\text{-}B|\geq 5$); thus, all configurations in which $|A\text{-}B|<5$, can be disqualified without a detailed simulation. Finally, the sample space must be small enough such that its *thorough* validation is computationally feasible. Thus, if the sample-space size cannot be sufficiently reduced (due to insufficient heuristics, etc.) other pruning techniques, such as the divide-and-conquer approach, must be incorporated into the sampling step (if possible).

### B. RETLab Framework

Fig. **5** illustrates the major components of *RETLab*. As seen in this figure, the inputs to the design problem are the target logic function and the set of available dyes and sites. The target logic function is described for *RETLab* in the form of an exciton flow graph (EFG) which is constructed based on the principles of RET logic and the functionality of the target function. In addition to these, the automated design flow also requires extra domain specific information which is classified into *Guidelines*, *Rules* and *Metrics*. These three classes of information are used by different components of *RETLab* to find the optimal RET network. Extraction of this information requires domain expertise and human intervention and cannot be automated.

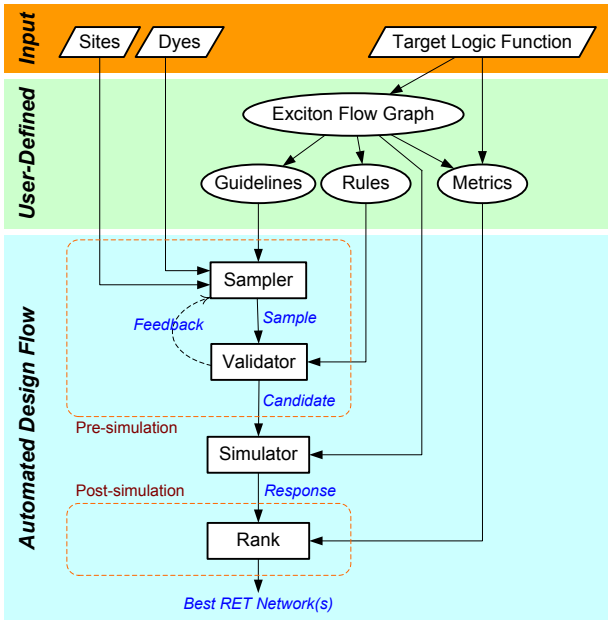


Fig. 5. Components of RETLab

## IV. Fast RET-Simulation Algorithm

In the *absence of saturation*, the kinetics of exciton migration in a RET network (which predicts its response) can be described by a system of ordinary differential equations (ODE) similar to Eq.1. However, an ODE system based on Eq.1 cannot accurately describe (discussed later) the behavior of RET networks with *saturated* nodes. For this reason, Monte-Carlo Simulation (MCS) is alternatively used to predict the behavior of such networks. Despite its flexibility, MCS has the drawback of being significantly slower than numerically solving ODE systems, and as a result, when used

in the automated design flow, MCS becomes the bottleneck, and imposes an upper bound on the total number of analyzed configurations per unit time, and possibly limits the maximum permitted size of the sample space. Therefore, to increase the simulation throughput and consequently enable a more extensive design space exploration, we developed a novel algorithm for RET calculation which – at the cost of higher memory consumption – is several orders of magnitude faster than MCS and yet highly precise.

### A. *Kinetics of RET in saturated networks*

For two reasons, Eq.1 fails to accurately describe the RET kinetics in a network with fully- or partially-saturated nodes: first, [D*] in this equation indicates only the size of the excited-population without providing any information about the *effective* excited-population which actually participates in RET. Second, in the cases where multiple donors compete for the same (shared) acceptor, the *effective* RET-rate constant from each co-donor to the acceptor, drops below its nominal rate constant (given by Eq.2), rendering $k_R$ values inaccurate. These two reasons are illustrated in Fig. 6 which compares a partially saturated acceptor (A) with an unsaturated one. In this figure, γ is the fraction of the excited D-population for which the acceptor is already excited, and hence cannot receive anymore excitons; therefore, the effective excited population is actually [D*]-γ. Further, since D is competing with another co-donor (i.e., B) for exciting A, some fraction of its excitons fails to hop to A, due to exciton collision; therefore, the effective RET-rate constant in this case is $k_R$-β.

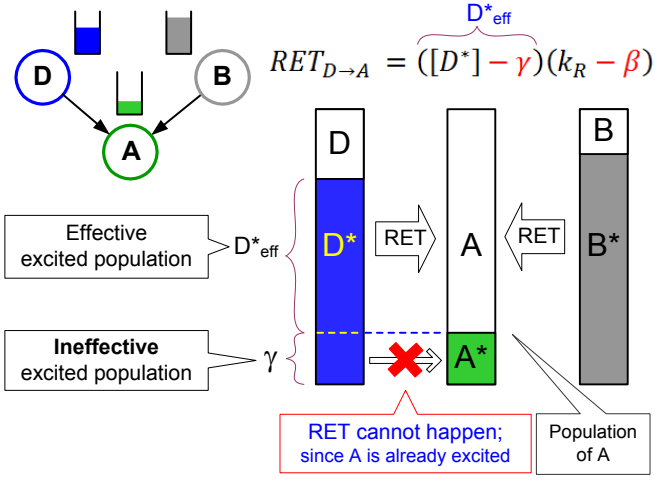


Fig. 6. Correction of Eq.1: $[D^*]k_R$ is written as $([D^*] - \gamma)(k_R - \beta)$

By adding the γ- and β-terms to the ODE of each RET pair (Fig. 6), the resulting ODE system can accurately describe the kinetics of exciton migration in the network even in the presence of saturation. Unfortunately, the values of γ(t) and β(t) are not known prior to solving the ODE system, rendering the conventional ODE solving techniques inapplicable. In the next section, we present a RET-specific algorithm to calculate the γ(t) and β(t) values, as well as the network response.

### B. *Algorithm*

To solve the aforementioned time-varying ODE system, we adopt a divide-and-conquer approach by partitioning the population into a number of sections each called a *stratum*. The stratification is performed based on the excitation status of nodes, for example in Fig. 7, the network has four nodes and therefore the population is partitioned into a total of sixteen ($2^4$) strata each representing one possible collective excitation status (only four strata, $\vartheta_1, \ldots, \vartheta_4$, are designated in the figure), e.g., $\vartheta_4$ represents the fraction of the population in which D and E are excited and F is unexcited. The size of all these strata is maintained in an array called *population profile* which is updated as the simulation proceeds.

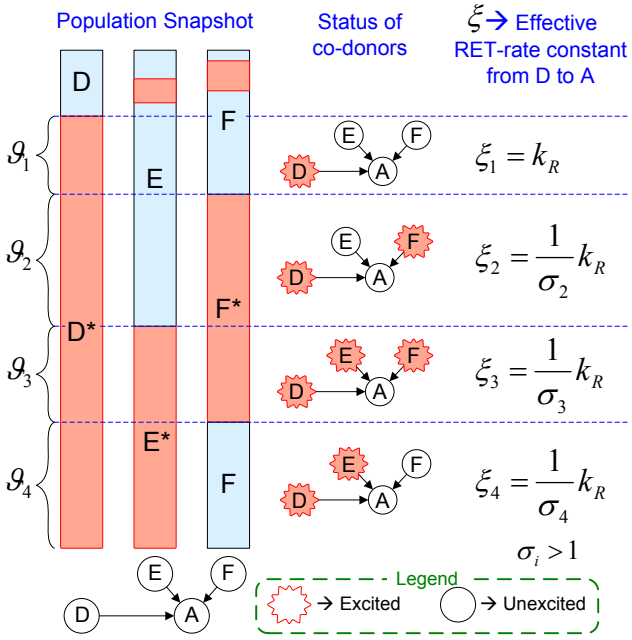


Fig. 7. Population Stratification: Only four strata are designated

The way that the population is stratified in this algorithm, enables us to easily obtain the γ values. Specifically, since the population of every node in each stratum is either fully excited or entirely unexcited, the donor-acceptor population overlap is either zero or 100% (i.e., γ=0 or γ=[D*]).

As shown in Fig. 8, after stratification and initialization, the simulation proceeds in small time steps ($\Delta t \to 0$) during each of which the system is assumed to be linear. In each time step, the response of each stratum is calculated separately, which is subsequently used to obtain the overall network response. Further, due to node-to-node exciton migration, the population distribution among the strata changes in each time step, thus, the population profile is updated with migration data before the simulation proceeds to the next time step.

Each stratum, proportional to its population, contributes to the overall network response at each time step. For instance, the instantaneous exciton transfer from D to A in Fig. 7 (denoted by $RET_{D\to A}$) is the weighted sum of the contributions of $\vartheta_1, \ldots, \vartheta_4$ in which D is excited, as expressed by the following formula, wherein $\vartheta_i$ denotes the population size of

stratum $i$ at time $t$ and $\xi_i$ denotes the effective RET-rate constant of the D→A pair in stratum $i$.

$$RET_{D\to A} = \sum_{i=1}^{4} \vartheta_i \xi_i = \vartheta_1\xi_1 + \vartheta_2\xi_2 + \vartheta_3\xi_3 + \vartheta_4\xi_4$$

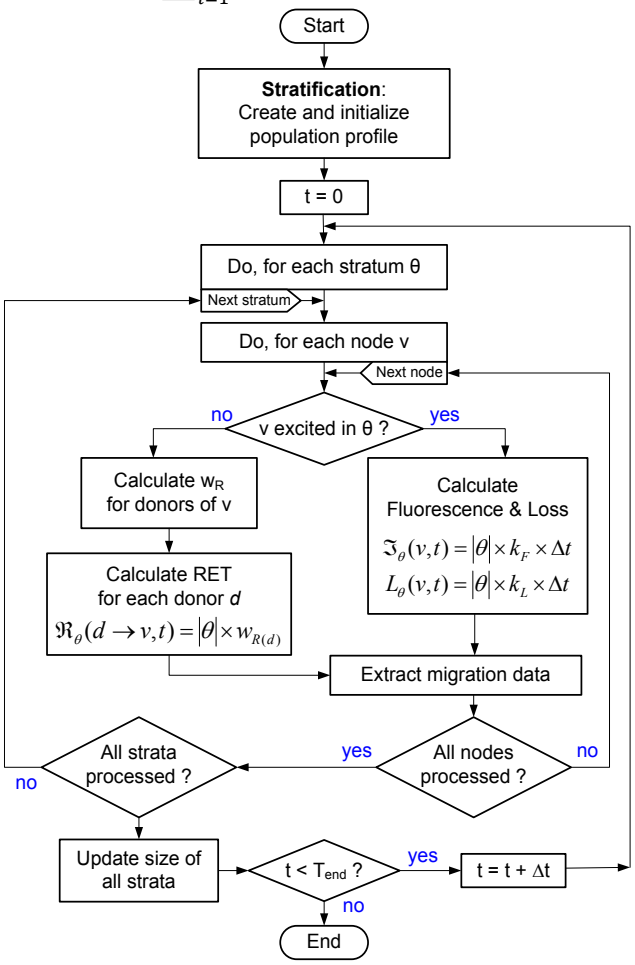


Fig. 8. Flowchart of the proposed RET calculation algorithm

### C. Calculation of Effective RET-rate Constants

The effective RET-rate constant ($k_R$-β in Fig. 6) of a RET pair equals its nominal rate constant (Eq.2) as long as its acceptor is *exclusively* excited by the donor (i.e., β=0). However, if the acceptor is shared by multiple co-donors, the effective RET-rate constant is reduced, due to the exciton collision caused by the competition among the co-donors. Therefore, to calculate the effective RET-rate constant of a RET pair in a given stratum we first obtain the probability of exciton collision at the acceptor in that stratum, and then we resolve the collision.

The exciton-collision probability depends on the number of participating co-donors and their strengths, which we refer to as *competition scenario*; for example, $D\bar{E}F$ is a scenario in which excitons at D and F (but not E) attempt to hop to the acceptor at the same time. The probability of this scenario is $P(D\bar{E}F) = P(D) \times \big(1 - P(E)\big) \times P(F)$ wherein P(D) denotes the probability that an exciton at D *attempts* to hop to the acceptor, which can in turn be calculated from $k_{R(D\to A)}$, the nominal RET-rate constant of D→A, as follows:

$$P(D) = \frac{\vartheta_i \times \Delta t \times k_{R(D\to A)}}{\vartheta_i} = \Delta t \times k_{R(D\to A)}$$

All different competition scenarios occur concurrently under each of which every co-donor receives a different share of successfully hopped excitons. Thus, the RET weight of co-donor $d$ – which we define as $w_{R(d)} = \xi(d) \times \Delta t$ – is the sum of $d$'s share of accepted excitons under all scenarios as expressed by Eq.3 in which P($s$) is the occurrence probability of scenario $s$ and $\Psi(s)$ is the donor's share of accepted excitons under $s$.

$$w_{R(d)} = \xi(d) \times \Delta t = \sum_{s \in E(d)} \mathrm{P}(s) \times \Psi(s) \qquad (3)$$

In this equation, E($d$) is the set of all scenarios in which $d$ attempts to hop; for example, Since F is not populated (excited) in stratum $\vartheta_4$ of Fig. 7, only D and E participate in the competition, and hence $E(\mathrm{D}) = \{DE, D\bar{E}\}$. Finally, the resolution function, Ψ, is calculated by $\Psi(s)=1/n$ wherein $n$ is the number of attempting co-donors, e.g., $\Psi(D\bar{E}) = 1$ and $\Psi(DE) = ½$.

## V. Evaluation and Discussion

To evaluate the performance of our RET simulation method, we simulated several RET networks with our method and also with a typical MCS method[13, 14], and compared the results in terms of precision and simulation speed (simulation length=8000ps). Both simulation algorithms were compiled with the same C++ compiler and ran on the same machine (64-bit Intel Core-i5 at 2.3 GHz).

While the error of both methods is affected by time resolution (Δt), the error in MCS with insufficient sampling cycles, is always higher than that of our method because the precision of a Monte-Carlo method is proportional to $\sigma/\sqrt{N}$ in which σ is the standard deviation of the underlying distribution and $N$ is the number of generated events[15]. Thus, as shown in Fig. **9**a, depending on the network, only after (tens of) millions of cycles, does the precision in MCS approach that of our method. Being deterministic, our method is highly precise (i.e., no variability) as it always yields the same result for the same input.

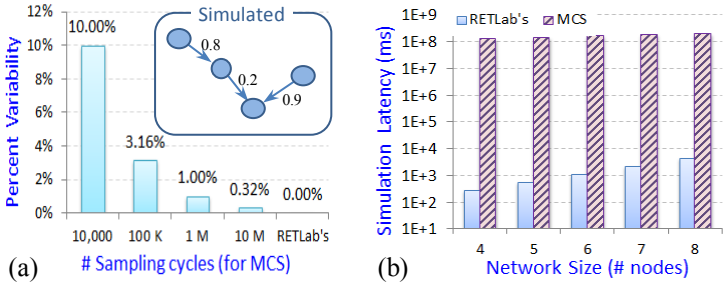


Fig. 9. MCS vs. our method: precision (a), and latency (b)

Fig. 9b shows the latency of our method versus that of MCS with ~ the same precision (~$10^7$ sampling cycles, Δt=1ps) for different network sizes (n). As seen in the figure, depending on n, our method is several orders of magnitude faster than MCS. For instance, when n=4 our method is ~one million times faster than MCS (latency: 140ms vs. ~40 hours).

### A. Why is our method faster?

The higher speed of our algorithm is due to the significantly fewer number of required iterations per time step ($\Delta t$); e.g., for a 4-node network, our method requires only 16 calculation cycles per $\Delta t$ (since $2^4$=16 strata), whereas MCS requires millions of sampling cycles per $\Delta t$. This speedup is achieved at the cost of limited scalability, since the population-profile vector in our algorithm grows exponentially with the number of network nodes. However, despite this limitation, our algorithm can still be employed in the design of large RET circuits, because they can often be broken down into smaller components each of which is optimized separately (as in the following example).

### B. Design Example: Sequence Detector

As a design example, we consider a wavelength sequence detector which detects a particular sequence of four symbols (i.e., wavelength-pairs). The circuit has 39 chromophores which is realized on a DNA grid with 192 available sites, and using 300 commercially-available dyes, yielding a design-space size of $\binom{300}{39} \times \binom{192}{39} \approx \sim 10^{90}$. Using conventional heuristics[4-6], the sample-space size was estimated to be larger than $\sim 10^{40}$, implying that these heuristics could not sufficiently prune the search space. Therefore, we broke the EFG of this circuit down into five distinct 3-chromophore components and used RETLab for each one separately. As depicted in Fig. 10, these five components included: AND gate, symbol detectors (three different symbols), and D-FlipFlop. The cited EFG-decomposition with spectral heuristics yielded a sample-space size of $\sim 10^8$ with a total candidate-space size of ~10,000 which was evaluated in ~ 27 minutes; whereas the same evaluation using MCS, even with a noticeably higher error (10%), takes more than 185 days to finish, highlighting the efficacy of our algorithm in improving the throughput of the automated RET network design process.

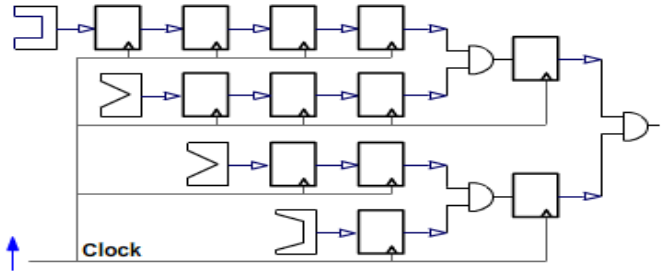


Fig. 10. Wavelength Sequence Detector – The circuit has 39 chromophores and is decomposed into five different 3-chromophore block types

## VI. Conclusion

The *real* functionality of a fabricated RET network usually deviates from its *desired* functionality due mainly to two reasons: 1- Undesired modified inter-chromophore distances imposed by the underlying nanostructure, 2- Undesired RET properties dictated by the molecular structure of chromophores. The desired functionality is described by an exciton-flow graph (EFG) which serves as the ideal model. Therefore, the automation problem is to find the configuration that yields the best behavioral match to the EFG.

Existing methods for RET network design are all *ad hoc* and limited to a particular functionality. Aside from lack of generalizability, due to their low throughput, these methods are incapable of efficiently exploring large design spaces within a limited design time.

In this work, we presented a *generic* RET-network design framework which has a higher throughput compared to ad hoc existing methods. The higher throughput of our design flow is enabled by avoiding unnecessary simulations, as well as employing a novel simulation algorithm which, in addition to being highly precise, is several orders of magnitude faster than conventional simulation methods. This higher throughput enables a more extensive exploration of larger design spaces, compared to the existing methods, making *RETLab* an efficient framework for optimizing RET circuit components and devices.

## References


[1] B. Valeur, *Molecular Fluorescence: Principles and Applications*. Weinheim: Wiley-VCH, 2002.

[2] M. D. Mottaghi and C. Dwyer, "Thousand-fold increase in optical storage density by polychromatic address multiplexing on self-assembled DNA nanostructures," *Adv Mater,* vol. 25, pp. 3593-8, Jul 12 2013.

[3] A. P. de Silva and S. Uchiyama, "Molecular Logic and Computing," *Nature Nanotechnology,* vol. 2, pp. 399-410, 2007.

[4] I. L. Medintz, A. R. Clapp, H. Mattoussi, E. R. Goldman, B. Fisher, and J. M. Mauro, "Self-assembled Nanoscale Biosensors Based on Quantum Dot FRET Donors," *Nature Materials,* vol. 2, pp. 630-638, 2003.

[5] J. K. Hannestad, P. Sandin, and B. Albinsson, "Self-assembled DNA Photonic Wire for Long-range Energy Transfer," *Journal of the American Chemical Society,* vol. 130, pp. 15889-15895, 2008.

[6] K. Boeneman, D. E. Prasuhn, J. B. Blanco-Canosa, P. E. Dawson, J. S. Melinger, M. Ancona, M. H. Stewart, K. Susumu, A. Huston, and I. L. Medintz, "Self-assembled Quantum Dot-sensitized Multivalent DNA Photonic Wires," *Journal of the American Chemical Society,* vol. 132, pp. 18177--18190, 2010.

[7] G. D. Scholes, G. R. Fleming, A. Olaya-Castro, and R. van Grondelle, "Lessons from Nature About Solar Light Harvesting," *Nat Chem,* vol. 3, pp. 763-774, 2011.

[8] E. Graugnard, D. L. Kellis, H. Bui, S. Barnes, W. Kuang, J. Lee, W. L. Hughes, W. B. Knowlton, and B. Yurke, "DNA-Controlled Excitonic Switches," *Nano Letters,* vol. 12, pp. 2117-2122, 2012.

[9] J. Zhu, L. Zhang, T. Li, S. Dong, and E. Wang, "Enzyme-Free Unlabeled DNA Logic Circuits Based on Toehold-Mediated Strand Displacement and Split G-Quadruplex Enhanced Fluorescence," *Adv Mater,* Feb 28 2013.

[10] C. Pistol, V. Mao, V. Thusu, A. R. Lebeck, and C. Dwyer, "Encoded multi-chromophore response for simulataneous label-free detection," *Small,* vol. 6, pp. 843-850, 2010.

[11] J. R. Lakowicz, *Principles of Fluorescence Spectroscopy*. New York: Kluwer Academic / Plenum Publishers, 1999.

[12] M. Beutler, K. Makrogianneli, R. Vermeij, M. Keppler, T. Ng, T. Jovin, and R. Heintzmann, "Satfret: Estimation of F*rster Resonance Energy Transfer by Acceptor Saturation," *European Biophysics Journal,* vol. 38, pp. 69--82, 2008.

[13] E. Wolfgang, H. Ruediger, and D. Heinz, "Structure-based calculation of multi-donor multi-acceptor fluorescence resonance energy transfer in the 4*6-mer tarantula hemocyanin," *Eur Biophys J,* vol. 33, pp. 386-395, 2004.

[14] P. Frederix, E. L. de Beer, W. Hamelink, and H. C. Gerritsen, "Dynamic Monte Carlo Simulations to Model FRET and Photobleaching in Systems with Multiple Donor-acceptor Interactions," *Journal Of Physical Chemistry B,* vol. 106, pp. 6793-6801, 2002.

[15] W. L. Dunn and J. K. Shultis, "Exploring Monte Carlo methods," *Choice: Current Reviews for Academic Libraries,* vol. 49, pp. 548-548, 2011.